ACCOUNTS
of chemical research

Solid-State NMR Studies of Biomineralization Peptides and Proteins

ADRIENNE ROEHRICH AND GARY DROBNY*

Department of Chemistry, University of Washington, Box 351700, Seattle, Washington 98195, United States

RECEIVED ON DECEMBER 3, 2012

CONSPECTUS

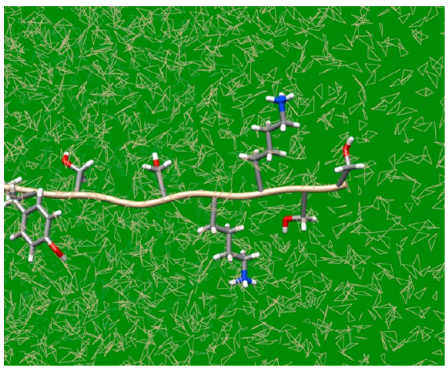

Nature has evolved sophisticated strategies for engineering hard tissues through the interaction of proteins, and ultimately cells, with inorganic mineral phases. This process, called biomineralization, is how living organisms transform inorganic materials such as hydroxyapatite, calcite, and silica into highly intricate and organized structures. The remarkable material properties of shell, bone, and teeth come from the activities of proteins that function at the organic–inorganic interface. A better understanding of the biomolecular mechanisms used to promote or retard the formation of mineral-based structures could provide important design principles for the development of calcification inhibitors and promoters in orthopedics, cardiology, urology, and dentistry. With the knowledge of the structural basis for control of hard tissue growth by proteins, scientists could potentially develop materials using biomimetic principles with applications in catalysis, biosensors, electronic devices, and chromatographic separations, to name a few. Additionally, biomineralization also has potential applications in electronics, catalysis, magnetism, sensory devices, and mechanical design. Where man-made hard materials require the use of extreme temperatures, high pressure, and pH, biological organisms can accomplish these feats at ambient temperature and at physiological pH.

Despite the fact that many researchers want to identify and control the structure of proteins at material and biomineral interfaces, there is a decided lack of molecular-level structure information available for proteins at biomaterial interfaces in general. In particular, this holds for mammalian proteins that directly control calcification processes in hard tissue. The most fundamental questions regarding the secondary and tertiary structures of proteins adsorbed to material surfaces, how proteins catalyze the formation of biomineral composites, or how proteins interact at biomaterial interfaces remain unanswered. This is largely due to a lack of methods capable of providing high-resolution structural information for proteins adsorbed to material surfaces under physiologically relevant conditions.

In this Account, we highlight recent work that is providing insight into the structure and crystal recognition mechanisms of a salivary protein model system, as well as the structure and interactions of a peptide that catalyzes the formation of biosilica composites. To develop a better understanding of the structure and interactions of proteins in biomaterials, we have used solid-state NMR techniques to determine the molecular structure and dynamics of proteins and peptides adsorbed onto inorganic crystal surfaces and embedded within biomineral composites. This work adds to the understanding of the structure and crystal recognition mechanisms of an acidic human salivary phosphoprotein, statherin.

Introduction and Background

Biomineralization is the process by which living organisms control the formation of inorganic materials like hydroxyapatite, calcite, and silica into highly intricate and organized structures.[1] A better understanding of the biomolecular mechanisms used to promote or retard mineral growth could provide important design principles for the development of calcification inhibitors and promoters in orthopedics, cardiology, urology, and dentistry.[2,3] In addition to biomedical applications, current interest in biomineralization also derives from its potential applications in electronics, catalysis, magnetism, sensory devices, and mechanical design,[4−12] where in contrast to anthropogenic synthesis of hard materials, which requires extremes in temperature, pressure, and pH, biological organisms accomplish impressive feats of hard tissue engineering at ambient temperature and at physiological pH.

Published on the Web 08/09/2013 www.pubs.acs.org/accounts
10.1021/ar300321e

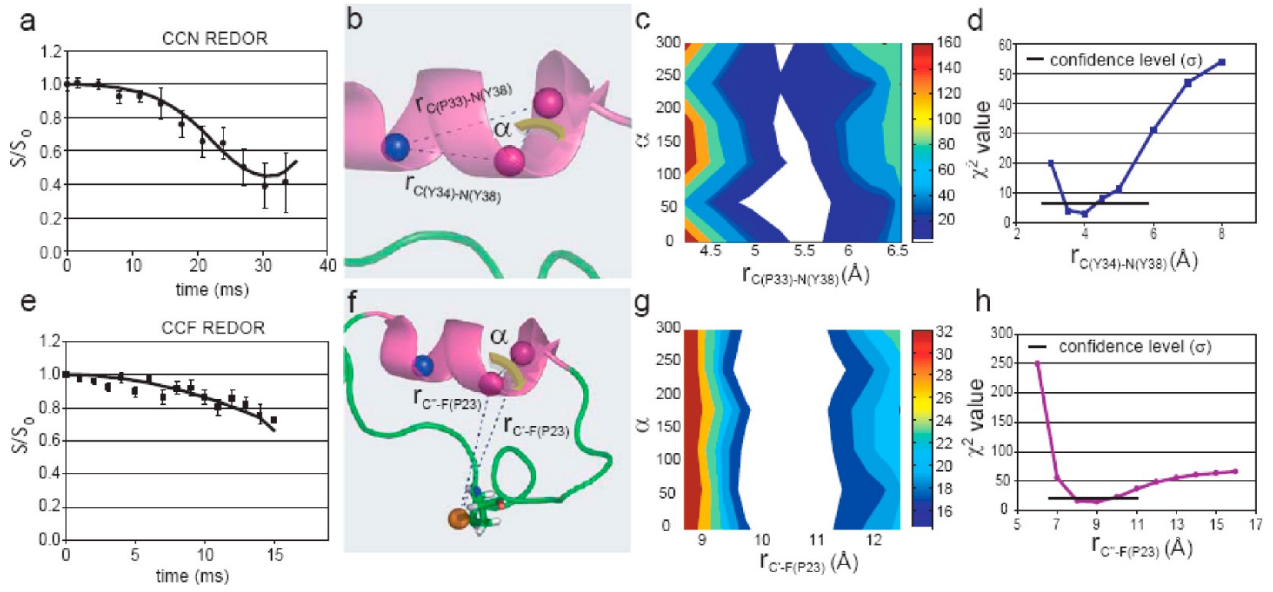

FIGURE 1. ssNMR data used to constrain Rosetta simulations. (a) ^{13}C signal decay (S/S_0) from recoupling of the $^{13}C-^{15}N$ dipolar couplings in a REDOR experiment. (b) Graphic visualization of dipolar interaction parameters in the C(P33)−C(Y34)−N(Y38) spin triad. (c) The contour plot of the parameter $\chi^2(r_{C(P33)-N(Y38)})$ for fits to CN REDOR data as a function of the angle α and the distance $r_{C(P33)-N(Y38)}$ and (d) graph of the $\chi^2(r_{C(Y34)-N(Y38)})$ function for fits to CN REDOR data plotted as a function of internuclear distance. (e) ^{13}C signal decay (S/S_0) from recoupling of the $^{13}C-^{19}F$ dipolar couplings in a REDOR experiment. The fits to these decay curves are used to extract the structural parameters. (f) Dipolar coupling parameters in the C(P33)−C(Y34)−F(P23) spin triad. Here, we denote the two carbons as C′ and C″ since they are indistinguishable in the ^{13}C spectrum. Plots of the (g) $\chi^2(r_{C'-F(P23)})$ function and (h) $\chi^2(r_{C''-F(P23)})$ function calculated from CF REDOR data plotted as a function of C−F distance.

In this Account, we discuss work that provides insight into the structure and crystal recognition mechanisms of an acidic human salivary phosphoprotein, statherin. In addition, we will show ssNMR data that give us the first molecular-level indication of how basic peptides derived from the biosilicification protein silaffin direct biosilica composite morphology.

Solid-State NMR Studies of Salivary Statherin on HAP Crystal Surfaces

Statherin is a small 5.38 kDa phosphoprotein, and the only salivary protein that has been found to inhibit both the nucleation and the growth of hydroxyapatite (HAP).[13−18] Statherin is expressed at its active length and post-translationally phosphorylated at serines 2 and 3.[19] It is then excreted by the sublingual and submaxillary salivary glands where it travels to the mouth. Statherin is composed of 43 amino acid residues with primary sequence H_2N-DpSpSE-EKFLRRIGRFGYGYGPYQPVPEQPLYPQPYQPQYQQYTF-COOH.

In addition to two phosphoserines (i.e., pS) statherin contains four aspartic/glutamic acid residues and four basic amino acids, almost all of which occur close to the N-terminus. Previous studies of statherin fragments by Nancollas and co-workers[20,21] showed that the N-terminal 15 amino acid fragment (SN-15, H_2N-DpSpSEEKFLRRIGRFG-COOH) is essential for binding to HAP crystal surfaces. Removal of the DpSpSE moiety (i.e., resulting in SN-11, EKFLRRIGRFG) reduces the HAP binding affinity by a factor of 4.5 compared with SN-15. Mutation of both phosphoserines to simple serine reduces the HAP binding affinity by a factor of almost nine. Mutation from serine to aspartic acid restores the binding affinity to 70% that of SN-15, indicating that the phosphoserine residues and acidic amino acid side chains are important for the binding of statherin to HAP. Initial ssNMR studies of HAP-bound statherin measured a number of torsion angles and internuclear distances within the N-terminal 15 amino acid segment of native statherin and within the 15 amino acid SN-15 peptide. These data indicate that the N-terminus HAP binding domain in HAP-adsorbed statherin is an α-helix.[22−24] Subsequent solid-state NMR studies of labeled HAP-bound statherin molecules yielded measurements of backbone torsion angles (residues 33−34) and i to (i + 4) carbonyl−amide distances (residues 34−38) indicating that the C-terminus receptor site for bacterial adhesion adopts an α-helical conformation on HAP crystal surfaces.[25] See Figure 1a−d.

To probe tertiary folding, we measured long-range distances between carbonyl carbons in the C-terminus (residues 33−34) and a fluorine nucleus incorporated into a proline ring (residue 23) showing that this motif closes back

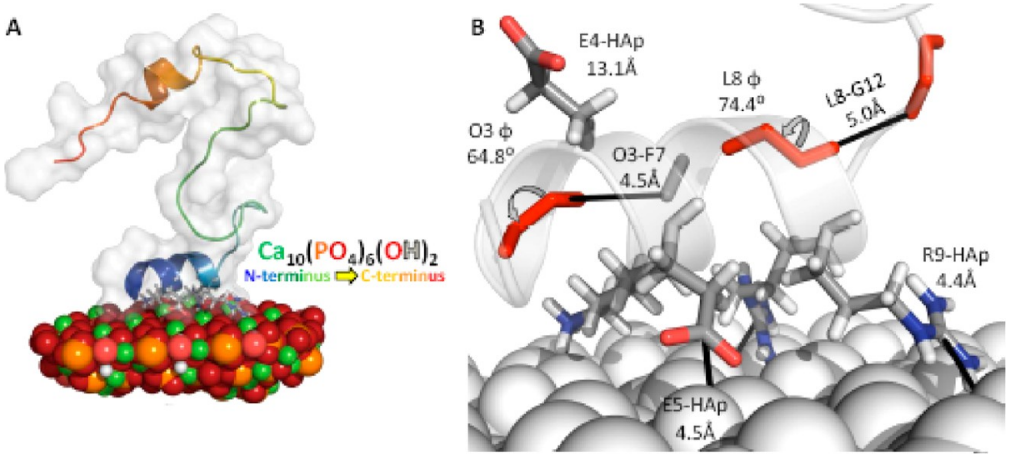

FIGURE 2. (A) Representative statherin structure on the 001 face of hydroxyapatite from the final phase of ssNMR-constrained RosettaSurface refinement. Opacity represents statherin's molecular shape; ribbons represent regions of helical structure. (B) individual amino acid side chains within the N-terminus that interact with the surface are shown as stick models with distances indicated between side chain ^{13}C or ^{15}N spins and ^{31}P surface spins. Reproduced from ref 27. Copyright 2010 Elsevier.

onto the protein's proline-rich region (16−28) through a series of backbone turns. These results elucidated the structure of the region in the protein that is recognized by pathogens and provided data on the overall fold of the protein when it binds to its natural solid substrate, hydroxyapatite. Some of these ssNMR data are summarized in Figure 1e−h.

The total number of distances between nuclei within statherin that reflect secondary and tertiary structure in the HAP-bound protein together with distances between nuclear spins in protein side chains to ^{31}P spins in the HAP surface that reflect surface proximity and orientation is insufficient to fully constrain statherin's surface structure. However, the body of ssNMR-derived structural measurements can be used to guide a molecular modeling computation, which provides an experimentally constrained model of the HAP-bound structure of statherin. Professor Jeffrey Gray and coworkers at Johns Hopkins University have developed a novel algorithm (RosettaSurface.NMR) as part of the Rosetta molecular modeling package for modeling the interactions of proteins with HAP crystal surfaces (i.e., ref 26). The algorithm uses experimentally derived ssNMR distance data to guide calculation of the structure and orientation of HAP-bound statherin. With this combined computational−ssNMR approach, analysis was made at a sufficiently high resolution to begin understanding residue- and atom-specific contributions to the process of biomineralization and hard tissue formation. Results of the RosettaSurface calculation indicate that when adsorbed onto HAP crystals, statherin has a stable C-terminal helix and a helical N-terminal HAP-binding domain with a local helix axis oriented more or less perpendicular to the local surface normal, see Figure 2A.

This domain interacts with the HAP surface via both basic and acidic residues. Predicted by RosettaSurface[26−28] and confirmed by our ssNMR[29,30] and calorimetric measurements,[31,32] of three acidic and two phosphoserines within this binding helix, only pS3 and E5 interact directly with the HAP surface, while basic residues K6, R9, R10, and perhaps R13 interact directly with phosphate oxygen triad groups within the HAP surface.[26−28] See Figure 2B.

To explore preferential face binding, RosettaSurface.NMR calculations were performed on five stable HAP crystal faces: 001, 010, 101, and two differentially terminated 100 faces (100-T1 and 100-T2), for a range of values of *w*, the parameter that weights ssNMR experimental constraints in the Rosetta Surface energy functional. Resulting calculations, shown in Figure 3, right, indicate significantly greater congruency at three of five tested HAP crystal surfaces, suggesting some specificity. One of the preferred faces is 001, the kinetically favored growth plane of HAP[33−36] and a face to which fluorescence microscopy experiments show HAP regulation proteins like statherin adhere.[35]

Our studies show that the basis for statherin's preferential face binding is the complementarity between the patterns of open phosphate oxygen triads (i.e., POTs) and the relative positions of side chains in statherin's N-terminal binding domain. Figure 3B−F delineate the smallest periodic pattern of POT's used to determine on each HAP crystal face the trends in $E_{constraint}$ with *w*. POT patterns on the 001 and 010 faces best facilitate simultaneous binding of E5, K6, R9, and R10. At the 100-T1 surface, binding via statherin's basic

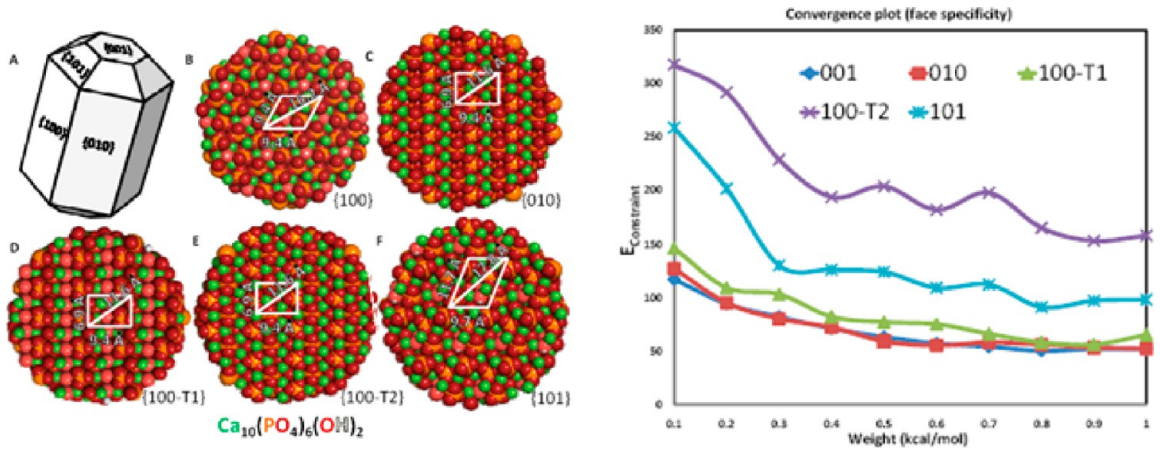

FIGURE 3. (A–G, left) Stable HAP crystal faces used to calculate statherin structures and binding specificity. (right) NMR constraint energy, $E_{constraint}$, plotted as a function of weighting parameter *w* and HAP face. Reproduced from ref 27. Copyright 2010 Elsevier.

residues is preferred at the expense of binding via E5. The 101 surface has a unique POT geometry, whose dimensions are larger than other surfaces used for these predictions. Binding via basic residues and E5 are compromised at the 101 surface. The 100-T2 surface is identical to the 010 surface with the addition of a calcium atom deposited into each phosphate cluster. Binding via E5 is among the best at that the 100-T2 surface, but binding of basic residues is disproportionately low at this surface.

Solid-State NMR Studies of Biosilicification Peptides

Silica-based materials find numerous applications in insulators, coatings, cosmetics, catalysis, and sensors[37−40] so nature-inspired methods for controlled silica morphogensis have been studied widely.[41] Diatoms, a unicellular microalgae, take in silicon as silicic acid ($Si(OH)_4$) and catalyze its deposition as silica (SiO_2), incorporating it into their cell walls, which become a mixture of organic material and self-produced silica. Proteins play an important role in the regulation of silica formation in diatoms. One of the most widely studied silica-regulating proteins is silaffin from the species *Cylindrotheca fusiformis*.[42−46] It is hypothesized that within the diatom, silaffins self-assemble into a matrix, which serves as a template for silica deposition. In vitro and in the absence of additional organizing components, addition of silaffins to silicic acid solutions results in the formation of silica nanospheres.[42]

The primary structure of the silaffin protein has been determined and displays a highly repetitive peptide sequence from residues 108 to 271, broken into homologous repeats R1−R7. Particular focus has been paid to the R5 sequence (SSKKSGSYSGSKGSKRRIL) because this peptide shows in vitro silica nanosphere formation activity that is similar to the parent silaffin but occurs at neutral pH and without the need for the post-translational modification of serines and lysines.[47−49] Elucidating the structure of R5 within a biosilica composite is a valuable step toward understanding how small peptides direct the formation of silica structures and thus mimic the behavior of biosilicification proteins like silaffin. Here we demonstrate the use of solid-state ^{13}C two dimensional magic angle spinning (2D MAS) NMR to probe directly structural features of the R5 peptide within a biosilica composite.

Figure 4 displays a SEM image obtained from the precipitation of silica from a silicic acid solution in the presence of the R5 peptide. The SEM images show that the silica precipitates are approximately spherical with diameters of 500−750 nm. The size and morphologies of these particles are consistent with those observed for precipitates formed by native silaffin proteins.[42] Spectrophotometric measurements of the supernatant peptide solution along with gravimetric analysis of the resulting solid indicate that the precipitates are typically 25−30% peptide by weight, also in agreement with reported R5−silica composite compositions reported in the literature.[48]

Prior studies of surface-adsorbed biomineralization proteins like statherin and amelogenin[27,29,30,50−53] were conducted with standard solid-state NMR dipolar recoupling pulse sequences applied as one-dimensional experiments. The high abundance of R5 peptide within the biosilica composite enables the efficient application of two-dimensional ssNMR techniques based on $^{13}C-^{13}C$ dipolar-assisted rotational resonance (DARR). Using DARR one is able to resolve and site specifically assign the ^{13}C spectrum of R5 in silica containing up to three uniformly enriched amino

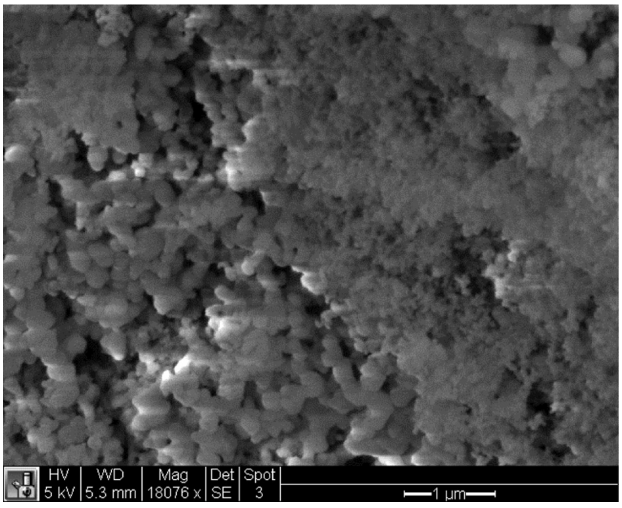

FIGURE 4. SEM image of the R5–silica coprecipitates, showing the formation of biosilica nanospheres with diameters of 500–750 nm.

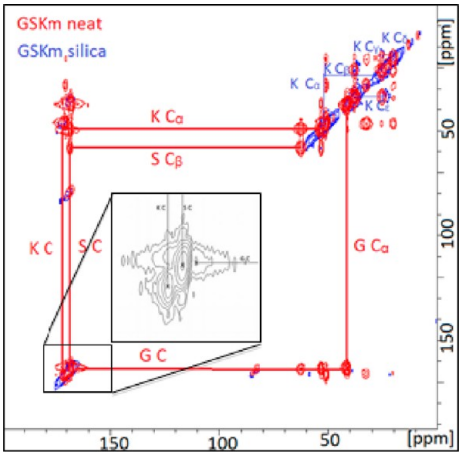

FIGURE 5. $^{13}C-^{13}C$ DARR spectrum of the R5 peptide SSKKSGSYSGSKGSKRRIL with uniformly enriched ^{13}C and ^{15}N amino acids incorporated at positions G10, S11, and K12. The DARR spectra of the neat R5 peptide and the biosilica incorporated peptide are superimposed to emphasize chemical shift changes that occur due to conformational differences between the free peptide and the peptide in the biosilica composite.

acids, requiring the study of seven isotopically enriched samples. With this approach virtually all the ^{13}C and ^{15}N spins in R5 can be assigned in silica, whereas from the 1D ^{13}C MAS spectrum of R5, only a few of the ^{13}CO peaks can be unambiguously assigned. Although the line widths are typically in the 1–3 ppm range, the large number of resolved cross-peaks allowed the average chemical shift to be determined to a much higher accuracy, typically 0.3–0.5 ppm.

Uniformly labeled ^{13}C and ^{15}N enriched amino acids are incorporated into the 19 amino acid R5 peptide via solid phase synthesis. The labeled samples are precipitated from silicic acid as a silica–R5 complex at 25 °C and pH 7.0 in a phosphate–citrate buffer. Two-dimensional ssNMR is performed on the lyophilized neat peptide sample and the dried biosilica composite sample. Dilution of the peptide within the composite causes lower signal-to-noise of those samples compared with the neat peptide samples. However, the peptide ^{13}C line widths are comparable for all samples. By 2D NMR methods, virtually all peaks in the R5 peptide and composite samples are resolved and assigned.

Figure 5 depicts the superimposed DARR spectra of the neat and biosilica associated R5 peptide with the G10, S11, and K12 residues uniformly enriched with ^{13}C and ^{15}N. A small subset of cross-peaks are labeled and assigned to demonstrate that all carbon resonances are resolved in the 2D spectrum. The solid vertical and horizontal lines in Figure 5 delineate networks of dipolar-coupled ^{13}C spins via cross-peaks, which allows assignment of the NMR peaks with known chemical shifts to specific ^{13}C spins within the R5 peptide. The neat sample shows the $^{13}C\alpha$ of the lysine and glycine and the $^{13}C\beta$ of the serine used to determine the exact peaks of each residue's carbonyl (black inset.) Note that the serine cross-peak indicated is the $^{13}C\beta$ to the carbonyl, illustrating the through space contact of DARR. A $^{13}C\alpha$ contact for the serine carbonyl and a $^{13}C\beta$ to $^{13}C\alpha$ serine contact are also present in the cross-peaks but not indicated explicitly in the figure.

The R5–biosilica composite sample is labeled to show the differentiation of the lysine side chain. In the composite, K12 showed less side chain ^{13}C chemical shift dispersion than for the same spins in the neat peptide. The shift dispersion of K12 is less than the other lysine side chain ^{13}C chemical shifts in the silica-associated peptide, which will be discussed later. The backbone $^{13}C\alpha$ has cross-peak contacts with $^{13}C\beta$, $^{13}C\gamma$, and $^{13}C\varepsilon$ where $^{13}C\beta$ and $^{13}C\gamma$ are stronger. $^{13}C\beta$ also interacts with $^{13}C\gamma$ and $^{13}C\varepsilon$. $^{13}C\gamma$ and $^{13}C\varepsilon$ also show cross-peaks indicating interaction. The $^{13}C\delta$ peak is weak at this mixing time; therefore cross-peaks to other side chain carbons do not appear in this spectrum.

Besides showing how the cross-peaks in a 2-D spectrum help elucidate otherwise ambiguous chemical shift assignments, this overlay also shows that there are perturbations in the chemical shifts occurring at some of the ^{13}C spins within the silica-associated R5 peptide. The perturbations in the chemical shift of the backbone ^{13}C spins (^{13}CO, $^{13}C\alpha$, $^{13}C\beta$), amide ^{15}N spins, and side chain ^{13}C spins observed when the R5 peptides is coprecipitated with silica from silicic acid solution are shown in Figure 6. Because the histograms indicate chemical shift changes (i.e., ΔCS) obtained by subtracting the chemical shift of the ^{13}C or ^{15}N spin in the neat

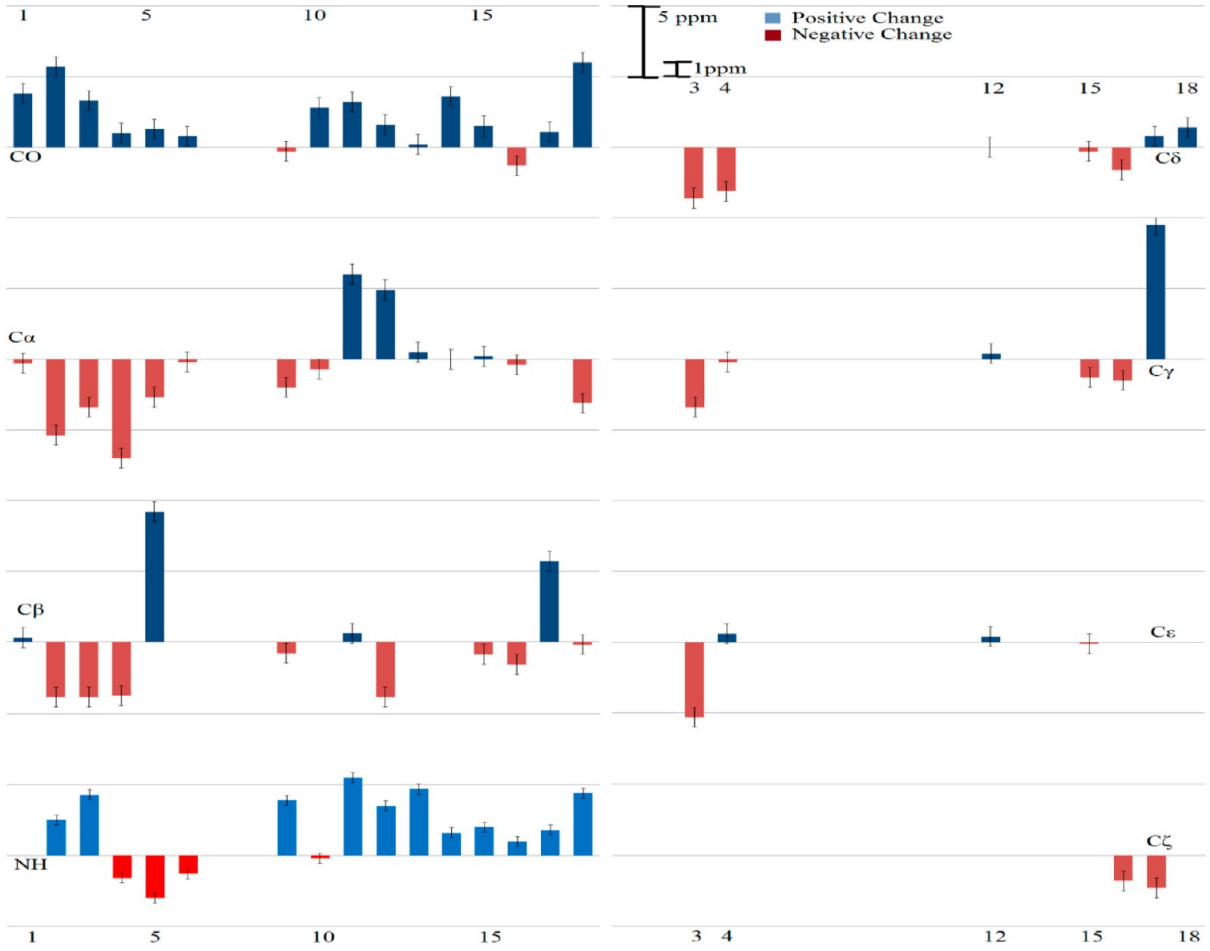

FIGURE 6. Perturbations of the chemical shifts of the ^{13}CO, ^{13}Cα, ^{13}Cβ, and ^{15}N amide nitrogen spins (left) and the side chain ^{13}C spins (right) in R5 coprecipitated with silica referenced to the native peptide. The R5 sequence is SSKKSGSYSGSKGSKRRIL, and the horizontal numbers indicate residue by sequential number. Blue bars indicate a positive change in shift, while red bars indicate a negative change.

peptide from the chemical shift of the same spin in the R5–silica complex, a positive ΔCS indicates that the chemical shift of a given spin has moved downfield, and a negative ΔCS indicates an upfield shift. While no simple trend of shifts for examining the secondary structure can be seen in the table,[54,55] significant perturbations in the chemical shifts of the backbone carbons and nitrogen are observed. These shifts are sensitive to the local environment backbone conformation, so the observed perturbations indicate a change of the backbone structure.

Figure 6 shows that the ^{13}Cγ, ^{13}Cδ, and ^{13}Cε spins of K3 are shifted upfield by several ppm in the R5–silica composite compared with the neat peptide; however, other ^{13}C spins in other lysine side chains in the R5–silica complex do not have large upfield shifts. Observed upfield ^{13}C shifts by the side chains in polylysine upon adsorption onto silica is attributed to the proximity of the side chain ^{13}C shift of lysine to the negatively charged silica surface in ^{13}C ssNMR studies.[56–58] This interaction has been also shown in ssNMR dipolar recoupling[40] and SFG[59] studies via the positively charged side chain functional groups, that is, the NH_3^+ group of the lysine. Therefore, perturbations in the ^{13}C chemical shifts of the side chains are likely to indicate contacts with silica.

The R16, R17, and I18 residues are also observed in Figure 6 to have chemical shift perturbations in their side chains. These residues fall into the C-terminal RRIL moiety, indicating a change in environment for these residues. The R16 chemical shifts of ^{13}Cγ, ^{13}Cδ, and ^{13}Cζ are moved upfield upon coprecipitation by silica, while R17 and I18 show downfield changes in side chain ^{13}C chemical shifts. The ^{13}Cζ of R17 is the exception. These perturbations are more complicated than the lysine interaction. Studies of silica precipitation by R5 mutants indicate the C-terminal RRIL moiety is necessary for silica formation activity.[47,48] R5 peptides with the RRIL moiety are observed by light scattering to form aggregates about 825 nm in diameter, and no aggregates are observed without the RRIL moiety. It has

been suggested that the pattern of arginine's positively charged guanidium groups in proximity to the hydrophobic leucine and isoleucine residues are likely involved in the micelle-like self-assembly.[20]

The pattern of chemical shift changes observed in R5 and portrayed in Figure 6 may therefore result from the formation of micellar-like peptide aggregates where positively charged amino acid side chains near the peptide N-terminus are exposed at the surface of the aggregate and interact with the surrounding silica matrix. This being the case, the side chain of K3 would clearly be most affected, K4 shows less significant perturbations, while K12 and K15 are buried within the aggregate and are removed from the silica matrix. The RRIL chemical shifts are likely due to the effect of peptide−peptide interactions, which are the basis for aggregate formation.

Figure 6 also shows that numerous chemical shift changes occur for the ^{15}NH, ^{13}CO, ^{13}Cα, and ^{13}Cβ spins throughout the R5 peptide upon formation of biosilica composites. Interpretation of these chemical shift changes is potentially complicated by the fact that the backbone ^{13}C chemical shifts are sensitive to conformational changes. However, given that biosilica composite formation is only observed in the presence of peptide aggregates and given that the orientation of the peptides in these aggregates likely leaves amino acid side chains beyond K3 largely removed from the silica matrix, we assume the backbone ^{13}C chemical shift changes observed beyond K3 are largely due to conformational changes.[56−58]

The self-assembly of peptides within biosilica-based nanostructures is widely studied.[60−63] Here we have shown how solid-state NMR can probe the structures of peptides within the biosilica composites, as well as the interaction between the peptide side chain and the mineral phase. In addition to work shown here, ^{15}N−^{29}Si REDOR used to quantify the proximity of the peptide to the silica phase[64] and secondary structure of the R5 peptide in silica determination are currently being explored. Further ssNMR studies will consider the nature of peptide assembly and its role in silica morphogenesis.

Conclusions

In this Account, we have shown how solid-state NMR techniques can provide information on the structure of proteins and peptides within biomineral composites together with information on protein−inorganic interactions to the level of atomic detail. Such information provides a clear picture of how proteins regulate the formation of these biomineral composites. In the case of statherin adsorbed onto HAP crystal surfaces, direct measurements of distances between ^{13}C and ^{15}N spins within the protein yield constraints for computational modeling of statherin's HAP-bound structure. Direct measurement of distances between nuclear spins in amino acid side chains of statherin and ^{31}P spins in the HAP surface, provide information on statherin's surface orientation and the basis for its face-selective binding. Chemical shift measurements obtained by two-dimensional ssNMR spectroscopic studies similarly provide information on the nature of peptide aggregates that provide templates for biosilica morphogenesis.

Further work is required to determine the extent to which the protein−mineral interactions derived from solid-state NMR studies of statherin−HAP and R5−silica composites varies for other protein−biomineral composites. Besides statherin the only other structure of a HAP-bound protein obtained to date is the ssNMR-derived structure of HAP-bound amelogenin, which plays an important role in the formation of tooth enamel.[51] In contrast to statherin, which has a well-structured helical HAP-binding domain and displays a high degree of face binding specificity, amelogenin has a high degree of structural dispersion on HAP to maximize surface coverage and somewhat less face binding specificity. With the two known structures for HAP binding proteins differing to such a significant degree, it is clear that more structures of surface-bound proteins need to be determined before a complete picture can emerge on how acidic proteins regulate HAP growth.

Solid-state NMR studies described here for biosilicification peptides mainly focused on studies of secondary structure in silica, but ssNMR methods are ideally suited to determining the structures of protein assemblies. To augment the qualitative chemical shift information presently in Figure 6, ^{13}C−^{29}Si and ^{15}N−^{29}Si REDOR experiments can be used to define quantitatively the interactions of the surrounding silica matrix with R5 peptide side chains. Dipolar recoupling ssNMR techniques applied to selectively ^{13}C-enriched peptides are widely used to determine the nature of protein assemblies in amyloid fibrils[65] and can be similarly applied to R5 peptides in silica matrices to determine the nature of protein aggregates in silica. Promising subjects for future ssNMR studies are silica-forming peptides whose mode of activity seems to differ from silaffins. An example is a class of silica-forming peptides called silacidins.[66] Although the RRIL moiety appears necessary for R5 self-assembly, which in turn is required for silica morphogensis, the *direct role* of such arginine-containing repeats has been questioned in the context of the precipitation of silica by silacidins. Wenzl

and co-workers[66] have shown that similar RRL repeats in silacidins act as linkers between otherwise polyanionic peptides. They propose that the linkers are removed to render completely anionic chains, which can bind polyamines. It is these complexes that are proposed to template silica. Another very promising direction for future exploration is the use of solid-state NMR to determine the role of protein assemblies in the formation of nanostructures based on nonbiological materials including TiO_2, GeO_2. Thus we are poised to apply ssNMR techniques to elucidate the structure of proteins in both naturally occurring biological composites as well as nonbiological nanostructures prepared using biologically inspired strategies.

We acknowledge Ariel Zane for sample preparation and Matt Power for data collection contributions to this work. Part of this work was conducted at the University of Washington NanoTech User Facility, a member of the NSF National Nanotechnology Infrastructure Network (NNIN). This work was supported by National Science Foundation Grant CHE 1219509 and National Institutes of Health Grant RO1 DE 12554.

BIOGRAPHICAL INFORMATION

Adrienne M. Roehrich received her Ph.D. in physical chemistry from the University of Nebraska, Lincoln, in 2010 on theoretical and experimental studies in solid-state NMR. She taught at the University of Nebraska, Omaha, and the College of St. Mary and conducted postdoctoral research at the University of Nebraska Medical Center. She is currently a postdoctoral researcher at the University of Washington studying the interaction of proteins and their associated biominerals using solid-state NMR.

Gary P. Drobny received his Ph.D. in Chemistry from the University of California, Berkeley, in 1981. He is a Professor of Chemistry and an Adjunct Professor of Physics at the University of Washington, Seattle. His research focuses on the application of solid-state NMR techniques to the study of the structure−function relationships of extracellular matrix proteins and in particular of biomineralization proteins in contact with their native mineral phases. He has authored over 150 articles including numerous NMR studies of proteins adsorbed onto biomineral and polymer surfaces.

FOOTNOTES

*Corresponding author. E-mail: drobny@chem.washington.edu.
The authors declare no competing financial interest.

REFERENCES

1 *Handbook of Biomineralization*; Wiley VCH: Weinheim, Germany, 2007.
2 Schoen, F. J.; Harasaki, H.; Kim, K. M.; Anderson, H. C.; Levy, R. J. Biomaterial-Associated Calcification: Pathology, Mechanisms, and Strategies for Prevention. *J. Biomed. Mater. Res.* **1988**, *22*, 11–36.
3 Coe, F. L.; Parks, J. H.; Asplin, J. R. The Pathogenesis and Treatment of Kidney Stones. *N. Engl. J. Med.* **1992**, *327*, 1141–1152.
4 Dickerson, M. B.; Sandhage, K. H.; Naik, R. R. Protein- and Peptide-Directed Syntheses of Inorganic Materials. *Chem. Rev.* **2008**, *108*, 4935–4978.
5 Gordon, R.; Losic, D.; Tiffany, M. A.; Nagy, S. S.; Sterrenburg, F. A. S. The Glass Menagerie: Diatoms for Novel Applications in Nanotechnology. *Trends Biotechnol.* **2009**, *27*, 116–127.
6 Losic, D.; Mitchell, J. G.; Voelcker, N. H. Diatomaceous Lessons in Nanotechnology and Advanced Materials. *Adv. Mater.* **2009**, *21*, 2947–2958.
7 Parker, A. R.; Townley, H. E. Biomimetics of Photonic Nanostructures. *Nat. Nanotechnol.* **2007**, *2*, 347–353.
8 Sanchez, C.; Arribart, H.; Giraud Guille, M. M. Biomimetism and Bioinspiration As Tools for the Design of Innovative Materials and Systems. *Nat. Mater.* **2005**, *4*, 277–288.
9 Cha, J. N.; Shimizu, K.; Zhou, Y.; Christiansen, S. C.; Chmelka, B. F.; Stucky, G. D.; Morse, D. E. Silicatein Filaments and Subunits from a Marine Sponge Direct the Polymerization of Silica and Silicones in Vitro. *Proc. Natl. Acad. Sci. U. S. A.* **1999**, *96*, 361–365.
10 Naik, R. R.; Whitlock, P. W.; Rodriguez, F.; Brott, L. L.; Glawe, D. D.; Clarson, S. J.; Stone, M. O. Controlled Formation of Biosilica Structures in Vitro. *Chem. Commun.* **2003**, 238–239.
11 Sandhage, K. H.; Allan, S. M.; Dickerson, M. B.; Gaddis, C. S.; Shian, S.; Weatherspoon, M. R.; Cai, Y.; Ahmad, G.; Haluska, M. S.; Snyder, R. L.; Unocic, R. R.; Zalar, F. M.; Zhang, Y.; Rapp, R. A.; Hildebrand, M.; Palenik, B. P. Merging Biological Self-Assembly with Synthetic Chemical Tailoring: The Potential for 3-D Genetically Engineered Micro/Nano-Devices (3-D GEMS). Intl. *J. Appl. Ceram. Technol.* **2005**, *2*, 317–326.
12 Schröfel, A.; Kratošová, G.; Bohunická, M.; Dobročka, E.; Vávra, I. Biosynthesis of gold nanoparticles using diatoms—silica-gold and EPS-gold bionanocomposite formation. *J. Nanopart. Res.* **2011**, *13*, 3207–3216.
13 Schlesinger, D. H.; Hay, D. I. Complete covalent structure of statherin, a tyrosine-rich acidic peptide which inhibits calcium phosphate precipitation from human parotid saliva. *J. Biol. Chem.* **1977**, *252*, 1689–1695.
14 Raj, P. A.; Marcus, E.; Sukumaran, D. K. Structure of human salivary histatin 5 in aqueous and nonaqueous solutions. *Biopolymers* **1998**, *45*, 51–67.
15 Schwartz, S. S.; Hay, D. I.; Schluckebier, S. K. Inhibition of Calcium Phosphate Precipitation by Human Salivary Statherin: Structure-Activity Relationships. *Calcif. Tissue Int.* **1992**, *50*, 511–517.
16 Campbell, A.; Ebrahimpour, A.; Perez, L.; Smesko, S.; Nancollas, G. The Dual Role of Polyelectrolytes and Proteins As Mineralization Promoters and Inhibitors of Calcium Oxalate Monohydrate. *Calcif. Tissue Int.* **1989**, *45*, 122–128.
17 Johnsson, M.; Richardson, C. F.; Bergey, E. J.; Levine, M. J.; Nancollas, G. H. The Effects of Human Salivary Cystatins and Statherin on Hydroxyapatite Crystallization. *Arch. Oral Biol.* **1991**, *36*, 631–636.
18 Jensen, J. L.; Lamkin, M. S.; Oppenheim, F. G. Adsorption of Human Salivary Proteins to Hydroxyapatite: A Comparison Between Whole Saliva and Glandular Salivary Secretions. *J. Dent. Res.* **1992**, *71*, 1569–1576.
19 Minaguchi, K.; Bennick, A. Invited Review: Genetics of Human Salivary Proteins. *J. Dent. Res.* **1989**, *68*, 2–15.
20 Wikiel, K.; Burke, E. M.; Perich, J. W.; Reynolds, E. C.; Nancollas, G. H. Hydroxyapatite Mineralization and Demineralization in the Presence of Synthetic Phosphorylated Pentapeptides. *Arch. Oral Biol.* **1994**, *39*, 715–721.
21 Richardson, C. F.; Johnsson, M.; Raj, P. A.; Levine, M. J.; Nancollas, G. H. The Influence of Histatin-5 Fragments on the Mineralization of Hydroxyapatite. *Arch. Oral Biol.* **1993**, *38*, 997–1002.
22 Shaw, W. J.; Long, J. R.; Dindot, J. L.; Campbell, A. A.; Stayton, P. S.; Drobny, G. P. Determination of Statherin N-Terminal Peptide Conformation on Hydroxyapatite Crystals. *J. Am. Chem. Soc.* **2000**, *122*, 1709–1716.
23 Shaw, W. J.; Long, J. R.; Campbell, A. A.; Stayton, P. S.; Drobny, G. P. A Solid State NMR Study of Dynamics in a Hydrated Salivary Peptide Adsorbed to Hydroxyapatite. *J. Am. Chem. Soc.* **2000**, *122*, 7118–7119.
24 Long, J. R.; Shaw, W. J.; Stayton, P. S.; Drobny, G. P. Structure and Dynamics of Hydrated Statherin on Hydroxyapatite as Determined by Solid-State NMR. *Biochemistry* **2001**, *40*, 15451–15455.
25 Goobes, G.; Goobes, R.; Schueler-Furman, O.; Baker, D.; Stayton, P. S.; Drobny, G. P. Folding of the C-Terminal Bacterial Binding Domain in Statherin upon Adsorption onto Hydroxyapatite Crystals. *Proc. Natl. Acad. Sci. U. S. A.* **2006**, *103*, 16083–16088.
26 Makrodimitris, K.; Masica, D. L.; Kim, E. T.; Gray, J. J. Structure Prediction of Protein−Solid Surface Interactions Reveals a Molecular Recognition Motif of Statherin for Hydroxyapatite. *J. Am. Chem. Soc.* **2007**, *129*, 13713–13722.
27 Masica, D. L.; Ash, J. T.; Ndao, M.; Drobny, G. P.; Gray, J. J. Toward a Structure Determination Method for Biomineral-Associated Protein Using Combined Solid- State NMR and Computational Structure Prediction. *Structure* **2010**, *18*, 1678–1687.
28 Masica, D. L.; Gray, J. J. Solution- and Adsorbed-State Structural Ensembles Predicted for the Statherin-Hydroxyapatite System. *Biophys. J.* **2009**, *96*, 3082–3091.
29 Ndao, M.; Ash, J. T.; Stayton, P. S.; Drobny, G. P. The Role of Basic Amino Acids in the Molecular Recognition of Hydroxyapatite by Statherin Using Solid State NMR. *Surf. Sci.* **2010**, *604*, L39–L42.

30 Ndao, M.; Ash, J. T.; Breen, N. F.; Goobes, G.; Stayton, P. S.; Drobny, G. P. A 13C{31P} REDOR NMR Investigation of the Role of Glutamic Acid Residues in Statherin- Hydroxyapatite Recognition. *Langmuir* **2009**, *25*, 12136–12143.

31 Goobes, R.; Goobes, G.; Shaw, W. J.; Drobny, G. P.; Campbell, C. T.; Stayton, P. S. Thermodynamic Roles of Basic Amino Acids in Statherin Recognition of Hydroxyapatite. *Biochemistry* **2007**, *46*, 4725–4733.

32 Goobes, R.; Goobes, G.; Campbell, C. T.; Stayton, P. S. Thermodynamics of Statherin Adsorption onto Hydroxyapatite. *Biochemistry* **2006**, *45*, 5576–5586.

33 Barnett, B. L.; Strickland, L. C. Structure of disodium dihydrogen 1-hydroxyethylidenediphosphonate tetrahydrate: a bone growth regulator. *Acta Crystallogr.* **1979**, *B35*, 1212–1214.

34 Margolis, H. C.; Beniash, E.; Fowler, C. E. Role of Macromolecular Assembly of Enamel Matrix Proteins in Enamel Formation. *J. Dent. Res.* **2006**, *85*, 775–793.

35 Simmer, J. P.; Fincham, A. G. Molecular Mechanisms of Dental Enamel Formation. *Crit. Rev. Oral Biol. Med.* **1995**, *6*, 84–108.

36 Zhan, J.; Tseng, Y. H.; Chan, J. C. C.; Mou, C. Y. Biomimetic Formation of Hydroxyapatite Nanorods by a Single-Crystal-to-Single-Crystal Transformation. *Adv. Funct. Mater.* **2005**, *15*, 2005–2010.

37 Neville, F.; Broderick, M. J. F.; Gibson, T.; Millner, P. A. Fabrication and Activity of Silicate Nanoparticles and Nanosilicate-Entrapped Enzymes Using Polyethyleneimine As a Biomimetic Polymer. *Langmuir* **2010**, *27*, 279–285.

38 Pouget, E.; Dujardin, E.; Cavalier, A.; Moreac, A.; Valery, C.; Marchi-Artzner, V.; Weiss, T.; Renault, A.; Paternostre, M.; Artzner, F. Hierarchical Architectures by Synergy between Dynamical Template Self-Assembly and Biomineralization. *Nat. Mater.* **2007**, *6*, 434–439.

39 Kent, M. S.; Murton, J. K.; Zendejas, F. J.; Tran, H.; Simmons, B. A.; Satija, S.; Kuzmenko, I. Nanosilica Formation at Lipid Membranes Induced by the Parent Sequence of a Silaffin Peptide. *Langmuir* **2008**, *25*, 305–310.

40 Cha, J. N.; Stucky, G. D.; Morse, D. E.; Deming, T. J. Biomimetic Synthesis of Ordered Silica Structures Mediated by Block Copolypeptides. *Nature* **2000**, *403*, 289–292.

41 Betancor, L.; Luckarift, H. R. Bioinspired Enzyme Encapsulation for Biocatalysis. *Trends Biotechnol.* **2008**, *26*, 566–572.

42 Kröger, N.; Deutzmann, R.; Sumper, M. Polycationic Peptides from Diatom Biosilica That Direct Silica Nanosphere Formation. *Science* **1999**, *286*, 1129–1132.

43 Kröger, N.; Lorenz, S.; Brunner, E.; Sumper, M. Self-Assembly of Highly Phosphorylated Silaffins and Their Function in Biosilica Morphogenesis. *Science* **2002**, *298*, 584–586.

44 Poulsen, N.; Kröger, N. Silica Morphogenesis by Alternative Processing of Silaffins in the Diatom Thalassiosira pseudonana. *J. Biol. Chem.* **2004**, *279*, 42993–42999.

45 Poulsen, N.; Sumper, M.; Kröger, N. Biosilica Formation in Diatoms: Characterization of Native Silaffin-2 and Its Role in Silica Morphogenesis. *Proc. Natl. Acad. Sci. U. S. A.* **2003**, *100*, 12075–12080.

46 Kröger, N.; Deutzmann, R.; Bergsdorf, C.; Sumper, M. Species-Specific Polyamines from Diatoms Control Silica Morphology. *Proc. Natl. Acad. Sci. U. S. A.* **2000**, *97*, 14133–14138.

47 Knecht, M. R.; Wright, D. W. Amine-Terminated Dendrimers as Biomimetic Templates for Silica Nanosphere Formation. *Langmuir* **2004**, *20*, 4728–4732.

48 Knecht, M. R.; Wright, D. W. Functional Analysis of the Biomimetic Silica Precipitating Activity of the R5 Peptide from *Cylindrotheca fusiformis*. *Chem. Commun.* **2003**, 3038–3039.

49 Rodríguez, F.; Glawe, D. D.; Naik, R. R.; Hallinan, K. P.; Stone, M. O. Study of the Chemical and Physical Influences upon in Vitro Peptide-Mediated Silica Formation. *Biomacromolecules* **2004**, *5*, 261–265.

50 Goobes, G.; Goobes, R.; Shaw, W. J.; Gibson, J. M.; Long, J. R.; Raghunathan, V.; Schueler-Furman, O.; Popham, J. M.; Baker, D.; Campbell, C. T.; Stayton, P. S.; Drobny, G. P. The Structure, Dynamics, And Energetics of Protein Adsorption—Lessons Learned from Adsorption of Statherin to Hydroxyapatite. *Magn. Reson. Chem.* **2007**, *45*, S32–S47.

51 Masica, D. L.; Gray, J. J.; Shaw, W. J. Partial High-Resolution Structure of Phosphorylated and Non-phosphorylated Leucine-Rich Amelogenin Protein Adsorbed to Hydroxyapatite. *J. Phys. Chem. C* **2011**, *115*, 13775–13785.

52 Shaw, W. J.; Ferris, K. Structure, Orientation, and Dynamics of the C-Terminal Hexapeptide of LRAP Determined Using Solid-State NMR. *J. Phys. Chem. B* **2008**, *112*, 16975–16981.

53 Shaw, W. J.; Ferris, K.; Tarasevich, B.; Larson, J. L. The Structure and Orientation of the C-Terminus of LRAP. *Biophys. J.* **2008**, *94*, 3247–3257.

54 Kricheldorf, H. R.; Mueller, D. Secondary Structure of Peptides. 3. Carbon-13 NMR Cross Polarization/Magic Angle Spinning Spectroscopic Characterization of Solid Polypeptides. *Macromolecules* **1983**, *16*, 615–623.

55 Shoji, A.; Ozaki, T.; Saito, H.; Tabeta, R.; Ando, I. Conformational Characterization of Solid Polypeptides by Carbon-13 NMR Recorded by the Cross Polarization-Magic Angle Spinning Method: Conformation-Dependent Carbon-13 Chemical Shifts of Oligo- and Poly(γ-benzyl L-glutamates) and Sequential Copolymers of γ-Benzyl and γ-Methyl L-Glutamates and Qualitative Evaluation of Side-Chain Orientation. *Macromolecules* **1984**, *17*, 1472–1479.

56 Fernandez, V. L.; Reimer, J. A.; Denn, M. M. Magnetic Resonance Studies of Polypeptides Adsorbed on Silica and Hydroxyapatite Surfaces. *J. Am. Chem. Soc.* **1992**, *114*, 9634–9642.

57 Chiang, C.-H.; Liu, N.-I.; Koenig, J. L. Magic-Angle Cross-Polarization Carbon 13 NMR Study of Aminosilane Coupling Agents on Silica Surfaces. *J. Colloid Interface Sci.* **1982**, *86*, 26–34.

58 Saitô, H. Conformation-Dependent 13C Chemical Shifts: A New Means of Conformational Characterization as Obtained by High-Resolution Solid-State 13C NMR. *Magn. Reson. Chem.* **1986**, *24*, 835–852.

59 Mermut, O.; Phillips, D. C.; York, R. L.; McCrea, K. R.; Ward, R. S.; Somorjai, G. A. In Situ Adsorption Studies of a 14-Amino Acid Leucine-Lysine Peptide onto Hydrophobic Polystyrene and Hydrophilic Silica Surfaces Using Quartz Crystal Microbalance, Atomic Force Microscopy, and Sum Frequency Generation Vibrational Spectroscopy. *J. Am. Chem. Soc.* **2006**, *128*, 3598–3607.

60 Khripin, C. Y.; Pristinski, D.; Dunphy, D. R.; Brinker, C. J.; Kaehr, B. Protein-Directed Assembly of Arbitrary Three-Dimensional Nanoporous Silica Architectures. *ACS Nano* **2011**, *5*, 1401–1409.

61 Brutchey, R. L.; Morse, D. E. Silicatein and the Translation of its Molecular Mechanism of Biosilicification into Low Temperature Nanomaterial Synthesis. *Chem. Rev.* **2008**, *108*, 4915–4934.

62 Scheffel, A.; Poulsen, N.; Shian, S.; Kröger, N. Nanopatterned Protein Microrings from a Diatom That Direct Silica Morphogenesis. *Proc. Natl. Acad. Sci. U. S. A.* **2011**, *108*, 3175–3180.

63 Xu, H.; Wang, Y.; Ge, X.; Han, S.; Wang, S.; Zhou, P.; Shan, H.; Zhao, X.; Lu, J. R. Twisted Nanotubes Formed from Ultrashort Amphiphilic Peptide I3K and Their Templating for the Fabrication of Silica Nanotubes. *Chem. Mater.* **2010**, *22*, 5165–5173.

64 Ben Shir, I.; Kababya, S.; Amitay-Rosen, T.; Balazs, Y. S.; Schmidt, A. Molecular Level Characterization of the Inorganic−Bioorganic Interface by Solid State NMR: Alanine on a Silica Surface, a Case Study. *J. Phys. Chem. B* **2010**, *114*, 5989–5996.

65 Balbach, J. J.; Ishii, Y.; Antzutkin, O. N.; Leapman, R. D.; Rizzo, N. W.; Dyda, F.; Reed, J.; Tycko, R. Amyloid Fibril Formation by Aβ16−22, a Seven-Residue Fragment of the Alzheimer's β-Amyloid Peptide, and Structural Characterization by Solid State NMR. *Biochemistry* **2000**, *39*, 13748–13759.

66 Wenzl, S.; Hett, R.; Richthammer, P.; Sumper, M. Silacidins: Highly Acidic Phosphopeptides from Diatom Shells Assist in Silica Precipitation In Vitro. *Angew. Chem.* **2008**, *120*, 1753–1756.